Electrostatic Layer-by-Layer Assembled Au Nano particle/MWNT Thin Films: Microstructure, Optical Property, and Electrocatalytic Activity for Methanol Oxidation

ARTICLE *in* CHEMISTRY OF MATERIALS · JULY 2009

Impact Factor: 8.35 · DOI: 10.1021/cm900688r

4 AUTHORS, INCLUDING:

Seung Woo Lee
Yeungnam University
208 PUBLICATIONS **3,981** CITATIONS

SEE PROFILE

CHEMISTRY OF MATERIALS
Article

Chem. Mater. **2009,** *21,* 2993–3001 2993
DOI:10.1021/cm900688r

Electrostatic Layer-by-Layer Assembled Au Nanoparticle/MWNT Thin Films: Microstructure, Optical Property, and Electrocatalytic Activity for Methanol Oxidation

Junhyung Kim,[†,§] Seung Woo Lee,[†,‡] Paula T. Hammond,*[,‡] and Yang Shao-Horn*[,†,§,⊥]

[†]*Electrochemical Energy Laboratory and* [§]*Department of Mechanical Engineering and* [⊥]*Department of Materials Science and Engineering and* [‡]*Department of Chemical Engineering, Massachusetts Institute of Technology, Cambridge, Massachusetts 02139*

Received March 10, 2009. Revised Manuscript Received May 4, 2009

Gold nanoparticle/multiwall carbon nanotube (AuNP/MWNT) thin films were fabricated by using the layer-by-layer (LBL) assembly technique. The microstructure of the film was characterized by TEM and AFM, which showed that the MWNTs in the AuNP/MWNT LBL films are randomly entangled to form a dense network, in which the AuNPs are intercalated. The plasmonic properties and electrocatalytic activity of these films were studied as a function of number of bilayers. Surface plasmon resonance of the AuNP/MWNT films increased linearly and exhibited a red shift with increasing number of bilayers as a result of increasing sizes of the AuNP agglomerates in the films. The AuNP/MWNT films were electrochemically active toward methanol oxidation reaction in alkaline solution. Linear sweep voltammograms revealed a systematic increase in the methanol oxidation current with increasing number of bilayers. This work offers promise to the development of efficient electrodes based on metal nanoparticle/MWNT nanoassembly for electrochemical energy conversion devices such as alkaline fuel cells and biosensors.

Introduction

Advanced hybrid materials such as noble metal, or semiconductor nanoparticles dispersed on surface-functionalized carbon nanotubes (CNTs) are one of the most actively pursued research areas. Not only are these materials of great interest at the fundamental level because of their unique properties but they can also be employed for a wide range of applications such as catalysts,[1−3] optical and electronic devices,[4−6] and electrochemical energy conversion and storage.[7−10]

Gold nanoparticles (AuNPs) have been the focus of numerous investigations because of their novel size- and shape-dependence in the optical,[11−14] electronic[13,15−17] and catalytic properties.[18,19] For instance, AuNPs interact strongly with visible light through the resonant excitation of the collective oscillations of their conduction electrons.[20] As a result of these collective oscillations, the surface plasmon resonance bands of AuNPs are characteristic of the size, shape, nanoparticle composition, and interparticle distances as well as the surrounding environment.[11,21−26] In addition, supported AuNPs have

*Corresponding author. E-mail: hammond@mit.edu (P.T.H.); shaohorn@mit.edu (Y.S.-H.).

(1) Yoon, B.; Wai, C. M. *J. Am. Chem. Soc*. **2005**, *127*, 17174–17175.
(2) Pan, X. L.; Bao, X. H. *Chem. Commun*. **2008**, 6271–6281.
(3) Giordano, R.; Serp, P.; Kalck, P.; Kihn, Y.; Schreiber, J.; Marhic, C.; Duvail, J. L. *Eur. J. Inorg. Chem*. **2003**, 610–617.
(4) Teo, B. K.; Sun, X. H. *Chem. Rev*. **2007**, *107*, 1454–1532.
(5) Jackson, A. M.; Myerson, J. W.; Stellacci, F. *Nat. Mater*. **2004**, *3*, 330–336.
(6) Quake, S. R.; Scherer, A. *Science* **2000**, *290*, 1536–1540.
(7) Tian, Z. Q.; Jiang, S. P.; Liang, Y. M.; Shen, P. K. *J. Phys. Chem. B* **2006**, *110*, 5343–5350.
(8) Liao, S. J.; Holmes, K. A.; Tsaprailis, H.; Birss, V. I. *J. Am. Chem. Soc*. **2006**, *128*, 3504–3505.
(9) Hsin, Y. L.; Hwang, K. C.; Yeh, C. T. *J. Am. Chem. Soc*. **2007**, *129*, 9999–10010.
(10) Girishkumar, G.; Vinodgopal, K.; Kamat, P. V. *J. Phys. Chem. B* **2004**, *108*, 19960–19966.
(11) Kelly, K. L.; Coronado, E.; Zhao, L. L.; Schatz, G. C. *J. Phys. Chem. B* **2003**, *107*, 668–677.
(12) Link, S.; Beeby, A.; FitzGerald, S.; El-Sayed, M. A.; Schaaff, T. G.; Whetten, R. L. *J. Phys. Chem. B* **2002**, *106*, 3410–3415.
(13) Yang, Y. Y.; Chen, S. W. *Nano Lett*. **2003**, *3*, 75–79.
(14) Lee, D.; Donkers, R. L.; Wang, G. L.; Harper, A. S.; Murray, R. W. *J. Am. Chem. Soc*. **2004**, *126*, 6193–6199.
(15) Chen, S. W.; Ingram, R. S.; Hostetler, M. J.; Pietron, J. J.; Murray, R. W.; Schaaff, T. G.; Khoury, J. T.; Alvarez, M. M.; Whetten, R. L. *Science* **1998**, *280*, 2098–2101.
(16) Liu, H. J.; Mun, B. S.; Thornton, G.; Isaacs, S. R.; Shon, Y. S.; Ogletree, D. F.; Salmeron, M. *Phys. Rev. B* **2005**, *72*, 5.
(17) Balasubramanian, R.; Guo, R.; Mills, A. J.; Murray, R. W. *J. Am. Chem. Soc*. **2005**, *127*, 8126–8132.
(18) Valden, M.; Lai, X.; Goodman, D. W. *Science* **1998**, *281*, 1647–1650.
(19) Subramanian, V.; Wolf, E. E.; Kamat, P. V. *J. Am. Chem. Soc*. **2004**, *126*, 4943–4950.
(20) Kreibig, U.; Vollmer, M. Optical Properties of Metal Clusters; Springer: New York, 1995.
(21) Kim, J.; Lema, K.; Ukaigwe, M.; Lee, D. *Langmuir* **2007**, *23*, 7853–7858.
(22) Eustis, S.; El-Sayed, M. A. *Chem. Soc. Rev*. **2006**, *35*, 209–217.
(23) Su, K. H.; Wei, Q. H.; Zhang, X.; Mock, J. J.; Smith, D. R.; Schultz, S. *Nano Lett*. **2003**, *3*, 1087–1090.
(24) Sung, J.; Hicks, E. M.; Van Duyne, R. P.; Spears, K. G. *J. Phys. Chem. C* **2007**, *111*, 10368–10376.
(25) Atay, T.; Song, J. H.; Nurmikko, A. V. *Nano Lett*. **2004**, *4*, 1627–1631.
(26) Mulvaney, P. *Langmuir* **1996**, *12*, 788–800.

Published on Web 06/10/2009

been extensively investigated as a catalyst for CO oxidation[18,27,28] and the water gas shift reaction,[29−32] where size reduction of AuNPs leads to enhanced intrinsic activity.[33−35] Recently, Au nanoparticles have been studied for electrooxidation of small molecules such as CO and methanol.[36−38] However, assembling Au nanoparticles in nanostructured thin films with electronic and ionic conduction pathways for electrochemical applications remains a challenge.[39−41] Here, we investigate this possibility through the use of nanometer-sized AuNPs and a highly interconnected network of CNTs using electrostatic assembly methods.

Several studies have reported the morphological features and electrochemical properties of LBL thin films that consist of metal nanoparticles and polymer.[42−46] Multilayered AuNP thin films on aminosilane functionalized quartz slides were fabricated by Srinivasan et al.[43] using LBL assembly with poly(allylamine hydrochloride) (PAH), which showed when the AuNPs were closely packed on the entire surface of substrate, the particles began to agglomerate with each other and formed large clusters with number of assembled layers increasing. Nart and co-workers have reported a fabrication process of nanostructured films comprising AuNP-containing amine-terminated G4 PAMAM dendrimer and PVS (poly(vinylsulfonic acid)) through the LBL technique, where enhanced charge transfer kinetics in the presence of AuNPs is studied as a function of number of bilayers.[42] Alexeyeva and Tammeveski combined CNTs with AuNP in alternation with poly(diallyldimethylammonium chloride).[47] In each of these cases, the films formed included an organic polymer that enabled construction of uniform continuous films, in which electronic communication among nanoparticles was hampered by the presence of the insulating polymer, and access to the surfaces of the nanoscale elements utilized was fairly low for the same reasons. For instance, electronic conductivity of alkane dithiol linked self-assembled multilayered AuNP thin films was measured in the range of $\sim 1 \times 10^{-1}$ to $\sim 1 \times 10^{-3}$ S/cm for smaller than 10 nm core size of AuNPs.[39,48] Therefore, it is highly desirable to disperse metal NP catalysts on electronically conductive support to reduce ohmic resistance and facilitate charge transfer for electrochemical applications.

CNTs have been intensively studied for the development of functional nanostructured materials since their discovery in 1991.[49] Recent electrochemical studies have shown promise in the use of CNTs with unique properties, such as high electrochemically accessible surface area, good chemical stability, and excellent electronic conductivity, for electrodes in electrochemical applications.[50−52] However, it is well-known that the poor solubility of the CNTs in most solvents has greatly limited the investigation of CNTs and their applications. To overcome the solubility limitations in the aqueous system, we have modified the surfaces of CNTs by carboxylic acid, amine, and other derivative functional groups for positively and negatively charged CNTs.[50,53] It has been demonstrated that CNTs can be assembled with a range of polyions using LBL techniques to generate mechanically and electrochemically interesting materials systems.[54,55] We have recently shown that such MWNTs can be functionalized to achieve high charge density and that the resulting MWNTs can be assembled into thin films on ITO using a layer-by-layer (LBL) method.[56] These MWNT/MWNT LBL thin films exhibited electronic conductivity on the order of 10 S/cm and tunable charge storage in acidic solution as a function of number of bilayers.

In this paper, we extend the idea to the alternating assembly of positively charged 2-aminoethanethiol stabilized AuNPs (Au-$SC_2H_4NH_2$) and negatively charged carboxylic acid functionalized MWNTs (MWNT-COOH) on an organosilane modified ITO electrode using the LBL approach (Scheme1). The optical properties and electrocatalytic oxidation activity of methanol on the AuNP/MWNT films on the ITO substrate were studied as a function of number of bilayers. We address two important questions regarding the optical properties and electrocatalytic activity of the LBL thin films: (1) the

(27) Haruta, M.; Kobayashi, T.; Sano, H.; Yamada, N. *Chem. Lett.* **1987**, 405–408.
(28) Haruta, A. *Chem. Rec.* **2003**, *3*, 75–87.
(29) Rodriguez, J. A.; Liu, P.; Hrbek, J.; Evans, J.; Perez, M. *Angew. Chem., Int. Ed.* **2007**, *46*, 1329–1332.
(30) Tabakova, T.; Boccuzzi, F.; Manzoli, M.; Sobczak, J. W.; Idakiev, V.; Andreeva, D. *Appl. Catal., B* **2004**, *49*, 73–81.
(31) Liu, Z.-P.; Jenkins, S. J.; King, D. A. *Phys. Rev. Lett.* **2005**, *94*, 196102.
(32) Burch, R. *Phys. Chem. Chem. Phys.* **2006**, *8*, 5483–5500.
(33) Valden, M.; Pak, S.; Lai, X.; Goodman, D. W. *Catal. Lett.* **1998**, *56*, 7–10.
(34) Grunwaldt, J. D.; Baiker, A. *J. Phys. Chem. B* **1999**, *103*, 1002–1012.
(35) Liu, H. C.; Kozlov, A. I.; Kozlova, A. P.; Shido, T.; Iwasawa, Y. *Phys. Chem. Chem. Phys.* **1999**, *1*, 2851–2860.
(36) Maye, M. M.; Lou, Y. B.; Zhong, C. J. *Langmuir* **2000**, *16*, 7520–7523.
(37) Lou, Y. B.; Maye, M. M.; Han, L.; Luo, J.; Zhong, C. J. *Chem. Commun.* **2001**, 473–474.
(38) Burke, L. D.; Nugent, P. F. *Gold Bull.* **1998**, *31*, 39–50.
(39) Leibowitz, F. L.; Zheng, W. X.; Maye, M. M.; Zhong, C. J. *Anal. Chem.* **1999**, *71*, 5076–5083.
(40) Fendler, J. H. *Chem. Mater.* **1996**, *8*, 1616–1624.
(41) Chen, S. W. *J. Phys. Chem. B* **2000**, *104*, 663–667.
(42) Crespilho, F. N.; Zucolotto, V.; Brett, C. M. A.; Oliveira, O. N.; Nart, F. C. *J. Phys. Chem. B* **2006**, *110*, 17478–17483.
(43) Zhang, F. X.; Srinivasan, M. P. *J. Colloid Interface Sci.* **2008**, *319*, 450–456.
(44) Hojeij, M.; Su, B.; Tan, S. X.; Meriguet, G.; Girault, H. H. *Acs Nano* **2008**, *2*, 984–992.
(45) Shi, J.; Hu, Y. Q.; Hua, Y. X. *Electroanalysis* **2008**, *20*, 1483–1489.
(46) Srivastava, S.; Kotov, N. A. *Acc. Chem. Res.* **2008**, *41*, 1831–1841.
(47) Alexeyeva, N.; Tammeveski, K. *Anal. Chim. Acta* **2008**, *618*, 140–146.
(48) Brust, M.; Bethell, D.; Kiely, C. J.; Schiffrin, D. J. *Langmuir* **1998**, *14*, 5425–5429.
(49) Iijima, S. *Nature* **1991**, *354*, 56–58.
(50) Sun, Y. P.; Fu, K. F.; Lin, Y.; Huang, W. J. *Acc. Chem. Res.* **2002**, *35*, 1096–1104.
(51) Guldi, D. M.; Rahman, G. M. A.; Zerbetto, F.; Prato, M. *Acc. Chem. Res.* **2005**, *38*, 871–878.
(52) Trancik, J. E.; Barton, S. C.; Hone, J. *Nano Lett.* **2008**, *8*, 982–987.
(53) Zheng, M.; Jagota, A.; Semke, E. D.; Diner, B. A.; McLean, R. S.; Lustig, S. R.; Richardson, R. E.; Tassi, N. G. *Nat. Mater.* **2003**, *2*, 338–342.
(54) Taylor, A. D.; Michel, M.; Sekol, R. C.; Kizuka, J. M.; Kotov, N. A.; Thompson, L. T. *Adv. Funct. Mater.* **2008**, *18*, 3354–3354.
(55) Mamedov, A. A.; Kotov, N. A.; Prato, M.; Guldi, D. M.; Wicksted, J. P.; Hirsch, A. *Nat. Mater.* **2002**, *1*, 190–194.
(56) Lee, S. W.; Kim, B.-S.; Chen, S.; Shao-Horn, Y.; Hammond, P. T. *J. Am. Chem. Soc.* **2009**, *131*, 671–9.

morphological changes of the resulting films as a function of number of bilayers, including the variation in AuNP distribution and interparticle interactions with increasing number of bilayers; (2) the electrocatalytic activity of the AuNP/MWNT LBL thin films toward methanol oxidation with increasing number of bilayers. LBL assembly of metal nanoparticle/MWNT films not only provides an alternative way to prepare electrodes for electrocatalysis with varying layer thickness, but also potentially improves utilization and dispersion of catalyst NPs because of the high catalytic surface area of CNTs. This study allows for the investigation of the assembly and morphological characterization of the AuNP/MWNT thin films, and the electrocatalytic activity as it correlates to the number of bilayers, which is of interest for potential applications such as catalysts, biosensors, and electrochemical energy conversion and storage materials.

Experimental Section

Chemicals. Hydrogen tetrachloroaurate trihydrate ($HAuCl_4 \cdot 3H_2O$, reagent grade), sodium borohydride ($NaBH_4$, 99%), tetraoctylammonium bromide (Oct_4NBr, 98%), thionyl chloride ($SOCl_2$, 99%), 4-(dimethylamino)pyridine (DMAP, 99%), 2-aminoethanethiol ($NH_2C_2H_4SH$, 97%), sulfuric acid (H_2SO_4, 95%), nitric acid (HNO_3, 70%), (3-aminopropyl)triethoxysilane (APTES, 98%), HPLC-grade toluene, and ethanol were used as received from Aldrich. Polished float ITO glasses were purchased from Delta technologies, Ltd., (surface resistivity = 4−8 Ω cm^{-2}, size 0.7 cm × 5 cm × 0.07 cm). Ultra pure water was prepared from Milli-Q plus system (Millipore Co.), resistivity greater than 18 MΩ cm^{-2}. MWNTs (95% purity) prepared by a conventional CVD method were purchased from NANOLAB.

Synthesis of AuNPs. 2-Aminoethanethiolate gold nanoparticles (AuNPs) were prepared using ligand exchange reaction from as prepared aqueous soluble DMAP-AuNPs.[57,58] Briefly, for the preparation of DMAP-AuNPs and ligand exchange reaction, to a vigorously stirred solution of 1.09 g (2.0 mmol) of Oct_4NBr in 100 mL of toluene was added 0.35 g (0.89 mmol) of $HAuCl_4 \cdot 3H_2O$ in 30 mL of Milli-Q water. The water phase was quickly cleared, and the toluene solution became dark red as $AuCl_4^-$ was transferred into it. The aqueous phase was removed and 0.38 g (10.0 mmol) of $NaBH_4$ that had been dissolved in 25 mL of Milli-Q water was quickly added to the toluene solution with vigorous stirring. The solution mixture immediately became black, indicative of AuNPs formation. Stirring was continued for 30 min at room temperature. After removing the aqueous phase, the black organic phase was collected and washed five times with 200 mL of Milli-Q water. An aqueous 100 mL of 0.1 M DMAP solution was added to the as-prepared 100 mL of AuNPs toluene solution. Direct phase transfer across the organic/aqueous boundary was completed within 3 h without stirring or agitation. And then 50 mL of 2-aminoethanethiol solution (0.45 mM in 95% ethanol, pH 10) was added to as prepared 75 mL of DMAP-AuNPs solution with additional 75 mL of Milli-Q water. The solution became cloudy and changed color from dark-red to violet, then to violet-blue, as the ligand-exchange reaction occurred. The mixture was left to stand at room temperature overnight. The dark fine nanoparticles were separated by gentle centrifugation, the precipitated solid residue was then dissolved in a minimum volume of alkaline Milli-Q water (pH 9−10; 10% KOH). The resulting solution was loaded onto a Sephadex G-25−150 column and eluted with Milli-Q water (pH 9−10). The dark-red fraction was collected.

Preparation of Surface-Functionalized MWNTs. Commercial MWNTs were refluxed in a concentrated 3:1 (v/v) H_2SO_4 and HNO_3 mixture at 70 °C to prepare carboxylic-acid-functionalized MWNTs (MWNT-COOH), and then washed with Milli-Q water several times using a membrane filter (0.2 μm). Further purification of the solution was conducted by dialysis in Milli-Q water bath for 4 days to remove any byproducts and residuals during functionalization before LBL thin film preparation.

Preparation of APTES/ITO Electrode. The received commercial ITO glasses were placed in Milli-Q water for a day. The ITO glasses were sonicated for 10 min in an ultrasonic bath in each of the following solvents: soapy water, Milli-Q water, acetone, and ethanol, leading to the formation of a more hydrophilic surface (i.e., more active hydroxyl surface) on the ITO layer.[59,60] To obtain the APTES/ITO electrode, the slides were placed in 10% (v/v) APTES/ethanol solution overnight. The electrodes were rinsed with ethanol to remove loosely bound organosilane molecules and then dried with a stream of nitrogen. The APTES/ITO electrodes were heated at 100 °C for 10 min in air.[60] Successively prepared APTES/ITO electrodes were placed in pH 3.5 Milli-Q water for LBL thin film preparation.

AuNP/MWNT LBL Assembly. AuNP/MWNT LBL thin films were deposited on the positively charged APTES/ITO electrodes using a modified Carl Zeiss DS50 programmable slide stainer. Briefly, the substrate was first dipped into a precisely pH 3.5 adjusted negatively charged carboxylic-acid-functionalized MWNTs solution for 30 min; it was then dipped in three baths of Milli-Q water for 3, 1, and 1 min each to remove loosely bound MWNTs. The substrates were then exposed into a positively charged amine functionalized AuNPs solution (pH 3.0) for 30 min, and washed in three baths of Milli-Q water for 3, 1, and 1 min each. This cycle made one bilayer of AuNP/MWNT. The cycle was repeated to produce thin films with the desired number of bilayer (Scheme 1b). After LBL assemblies, substrates were annealed at 150 °C for 12 h in a vacuum oven (30 in Hg, Isotemp vacuum oven-model 281A).

Instrumentation

UV/Visible Spectroscopy. The UV/vis spectra of the samples were recorded on an Agilent 8453 UV/vis spectroscopy in the range of 300−1100 nm. A quartz cuvette with a 1 cm light path and thiolated AuNPs solution in H_2O was used as the optical characterization of the AuNPs. The optical spectra of a silanized ITO slide was used for blank and freshly prepared AuNP/MWNT LBL thin film on ITO were recorded by placing the thin films perpendicular to the beam in order to maintain the same experimental conditions for each measurement.

Zeta Potential Measurements. The zeta potential as a function of pH was measured using a Zeta PALS (Brookhaven Instrument Corp.) to determine the effect of surface charge in the thiolated AuNPs and carboxylic

(57) Gittins, D. I.; Caruso, F. *Angew. Chem., Int. Ed.* **2001**, *40*, 3001–3004.
(58) Rucareanu, S.; Gandubert, V. J.; Lennox, R. B. *Chem. Mater.* **2006**, *18*, 4674–4680.
(59) Zhang, J. D.; Kambayashi, M.; Oyama, M. *Electrochem. Commun.* **2004**, *6*, 683–688.
(60) Cheng, W. L.; Dong, S. J.; Wang, E. K. *Langmuir* **2002**, *18*, 9947–9952.

acid surface functionalized MWNTs solutions. The data were analyzed using standard procedures in the software provided with the instrument.

TEM and AFM. Transmission electron microscopy (TEM) images of AuNPs, MWNTs, and LBL thin film samples were obtained with a JEOL transmission electron microscope (JEOL-200CX). TEM grids of AuNPs, MWNTs, and LBL thin film were prepared on a 200 mesh lacey carbon-coated copper grid (200C-LC, Electron Microscopy Sciences) and drying in air before imaging. Surface topology of AuNP/MWNT LBL film on APTES/ITO electrode was examined using an AFM microscope (Digital Instruments EnviroScope, Veeco) in the tapping mode in air.

Electrochemical Measurements. All electrochemical experiments were carried out in a conventional three-electrode electrochemical cell by using a voltamaster potentiostat (Radiometer analytical, France). The working electrode was an AuNP/MWNT LBL thin film on the modified ITO glass. A platinum wire and a saturated calomel electrode (SCE) were used as counter electrode and reference electrode, respectively. All measurements were performed at room temperature. Nitrogen was purged in the solution 30 min before starting each electrochemical measurement. Cyclic voltammetry (CV) and linear sweep voltammetry (LSV) were measured between −0.2 and 0.6 V (vs SCE) at a scan rate of 20 mV/s. The reference electrode potential conversion from SCE to RHE is shown in the Supporting Information.

Results and Discussion

AuNP/MWNT LBL Film Preparation. 2-Aminoethanethiolated AuNPs were prepared in dilute aqueous solution as described in the experimental section. The surfaces of the AuNPs are covered by amine functional groups that could be protonated ($-NH_3^+$) over a broad acidic pH range after dissolving in Milli-Q water.[58] On the other hand, negatively charged MWNTs surfaces are covered with carboxylate anions ($-COO^-$) in aqueous solution.[56] To confirm this, zeta-potential measurements were performed for both AuNPs and MWNTs solutions. The zeta-potential values were obtained to be +34 mV (AuNPs) and −35 mV (MWNTs) at pH 3.0 and pH 3.5, respectively. This clearly shows that the surfaces of the AuNPs and MWNTs are positively and negatively charged with the pH of the solution.

As described in Scheme 1, the fabrication of the positively charged AuNP and the negatively charged MWNT LBL film on the APTES/ITO electrodes was carried out making use of a well-described multistep procedure, in which first the silane-modified ITO substrate was immersed into the solution of MWNTs and steps 1−4 were repeated until the desired LBL thin films were obtained. After deposition of the AuNP/MWNT thin film on the APTES/ITO electrode, the ITO electrode was additionally heated at 150 °C for 12 h in a vacuum oven, resulting

Scheme 1. (a) Procedure for the Preparation of APTES/ITO Substrate, (b) Illustration of Positively Charged AuNP and Negatively Charged MWNT LBL Thin Film Deposition Process

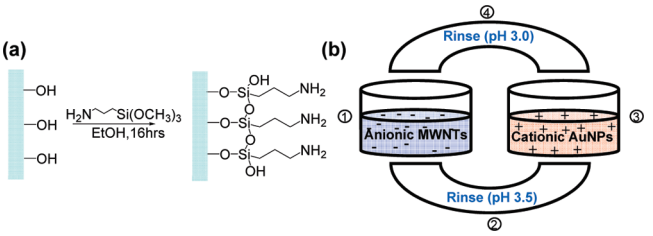

in the formation of amide bonds between amine-functionalized AuNPs and carboxylic acids on the MWNT surfaces.[56,61] There are also amide bonds formed between MWNT surfaces and the amino groups on the APTES/ITO substrate at the same temperature, which further increases the matrix adhesion and mechanical cohesion. TEM, AFM, UV/vis spectroscopy, and electrochemical measurements were conducted to characterize and evaluate the properties of LBL thin films in terms of the number of bilayers.

Microstructure Characterization of LBL Thin Films. The size and shape of the amine functionalized AuNPs were obtained by TEM. In order to obtain a good statistical analysis for the particle core size distribution, the core-size histogram was read from digitized photographic images using Scion Image Alpha 4.0.3.2 (www.scioncorp.com), and the value was confirmed with manual measurements. The gold nanoparticles in Figure 1a are spherical in shape and are monodisperse. The average core size is 3.4 ± 0.2 nm. TEM images of commercial and surface functionalized MWNTs (length 1−5 μm, outer diameter 15 ± 5 nm) are shown in the Supporting Information, Figure S1a and b. To understand the LBL film structure as a function of number of bilayers, we examined the size distribution and density of the AuNPs and orientation of the MWNTs using TEM and AFM (Figures 1 and 2).

The TEM images (Figure 1b−d) show 2, 4, and 7-bilayer AuNP/MWNT films and illustrate that successive LBL multicycle depositions of AuNPs and MWNTs on the APTES/ITO substrate lead to an increasing density of AuNPs and MWNTs while maintaining the same AuNPs core size. As shown in Figure 2a, empty surface patches are visible in the samples with relatively higher surface roughness (Figure 3a), which indicates that the multilayer films do not reach full surface coverage of AuNPs on the MWNT surfaces with bilayer number equal to or less than the seventh. The fact that the initial adsorption of multilayer films, in particular those consisting of nanoparticles, requires multiple adsorption cycles before complete surface coverage is achieved.[43,45] On the other hand, images a and b in Figure 2 display the AFM images of 7-bilayer and 13-bilayer AuNP/MWNT films on the APTES/ITO slide, respectively. The AuNPs adhere to the surfaces of the underlying oppositely charged MWNTs in the LBL film at each deposition step; the 7-bilayer film indicates a structure in which the MWNTs remain visibly articulated after the AuNP

(61) Harris, J. J.; DeRose, P. M.; Bruening, M. L. *J. Am. Chem. Soc.* **1999**, *121*, 1978–1979.

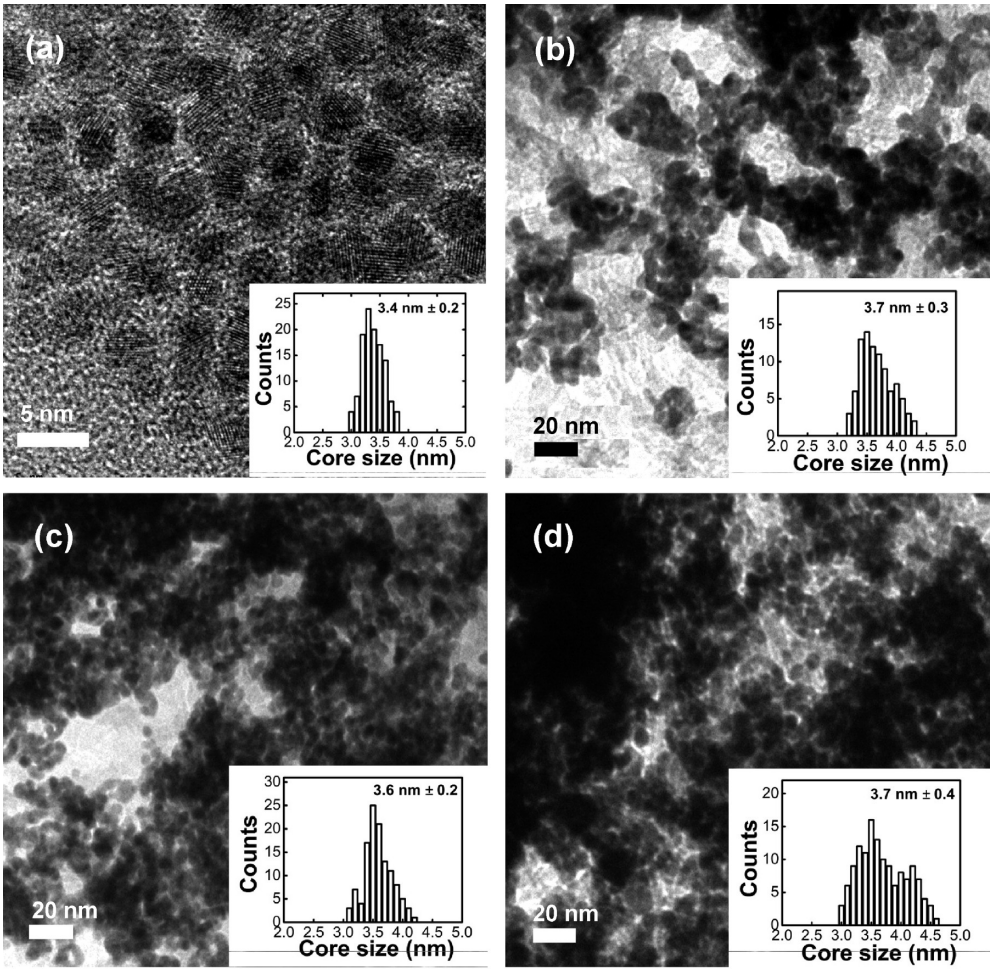

Figure 1. (a) TEM image and histogram of AuNPs core size. (b−d) TEM image and histogram of AuNP core sizes for AuNP/MWNT films with 2, 4, and 7 bilayers, respectively.

adsorption step, as shown in Figure 2a. The MWNTs in the LBL thin film are randomly arranged on the ITO substrate (Figure 2a); the randomly entangled orientation observed in Figure 2a is reminiscent of the all-MWNT films prepared in previous work.[56]

The AuNPs appear to be larger than 4 nm in Figure 2a because of the limited AFM tip radius. However, the height of the particles, whose measurement is not affected by the tip radius, is around 3−4 nm. Figure 3a contains the root-mean-squared (rms) roughness as a function of number of bilayers. It can be seen from the TEM and AFM results in Figures 1 and 2 and the roughness data in Figure 3a that the film is initially rough because of incomplete surface coverage and packing of nanoparticles and MWNTs. However, in Figures 2b and 3a, it is clear that the features of the MWNTs are no longer observed on the 13-bilayer film. rms roughness decreases with thicker LBL films, particularly between 7 and 13 bilayers, indicating that once the surface coverage of AuNPs is reached, the AuNPs begin to fully cover the surface of the MWNT film at each adsorption step and remain closely packed between the MWNT layers in subsequent cycles. The rms roughness above 13 bilayers is 7−8 nm, which suggests aggregation of Au nanoparticles in the film.

Figure 3b indicates the thickness as a function of number of bilayers as determined by profilometry. The data suggest two linear growth regimes for the LBL thin film. At low numbers of bilayers, the film grows at a slower rate as material is directed toward complete filling of surface voids, whereas above approximately 10 bilayer pairs, the film grows at a faster, but still linear, rate. It is at this point that the AuNPs are well-distributed over the MWNT surface. This kind of gradual increase in particle aggregation has been observed in previous work[43] for which a consistently increasing particle aggregate size was observed using AFM and UV−vis absorption. In this example, however, the system consisted of a polyelectrolyte alternated with the AuNP, thus yielding complete surface coverage in the first one to two bilayers; polyions are able to adsorb on larger numbers of surface sites to yield conformal coatings more readily than nanoscale objects. Here we observe that aggregation does not begin until after surface coverage is achieved following several cycles of deposition. Once full surface coverage of AuNPs is achieved, however, a more uniform film is produced, as shown in Figure 2b, and particle aggregation begins to occur in these systems with increasing bilayer pair.

Plasmonic Property of LBL Thin Films. Figure 4 demonstrates the optical absorbance of the AuNP/MWNT

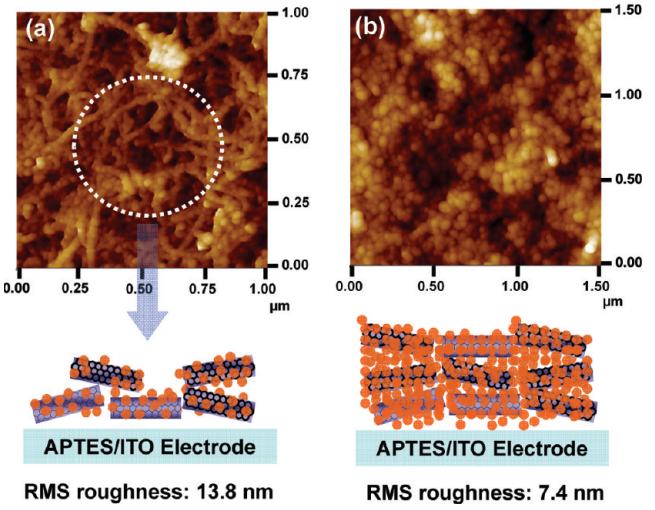

Figure 2. Representative AFM images of the AuNP/MWNT LBL thin films with (a) 7 bilayers (1 μm × 1 μm) and (b) 13 bilayers (1.5 μm × 1.5 μm) on the APTES/ITO substrate.

LBL thin films as a function of number of bilayers. Amine functionalized AuNPs (Figure 1a) in aqueous solution (pH 3.0) showed an absorption peak at about 520 nm, because of the collective oscillation of the electrons in the conduction band of the gold atoms, under optical excitation (see the Supporting Information, Figure S2). Figure 4a shows the optical spectra of the AuNP/MWNT LBL films built up on the APTES/ITO slide. The spectra show characteristic absorption bands at 320 nm and in the range of 570−610 nm corresponding to the absorption bands of functionalized MWNTs film and AuNPs, respectively. The absorbance at the surface plasmon resonance increased linearly with increasing number of bilayers (Figure 4b); this also confirmed the increase in film thickness by the LBL assembly technique.

In addition, the absorbance peak of MWNTs at 320 nm is gradually decreased with increased bilayer numbers, indicating the increased loading amount of AuNPs on the MWNT surface as shown in Figure 2b. It is interesting to

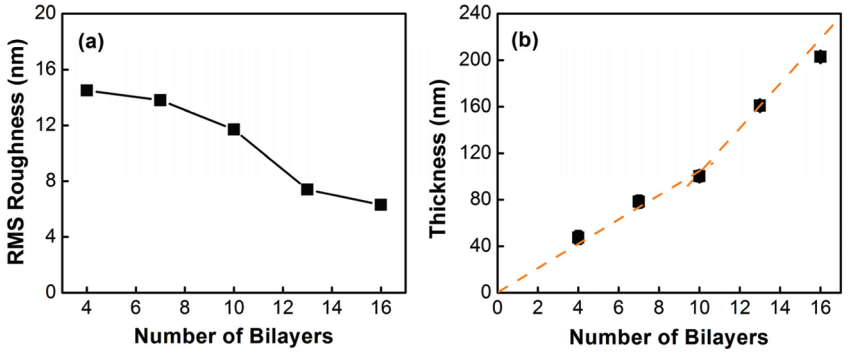

Figure 3. (a) rms roughness and (b) thickness of AuNP/MWNT LBL thin films as a function of number of bilayers on the APTES/ITO substrate.

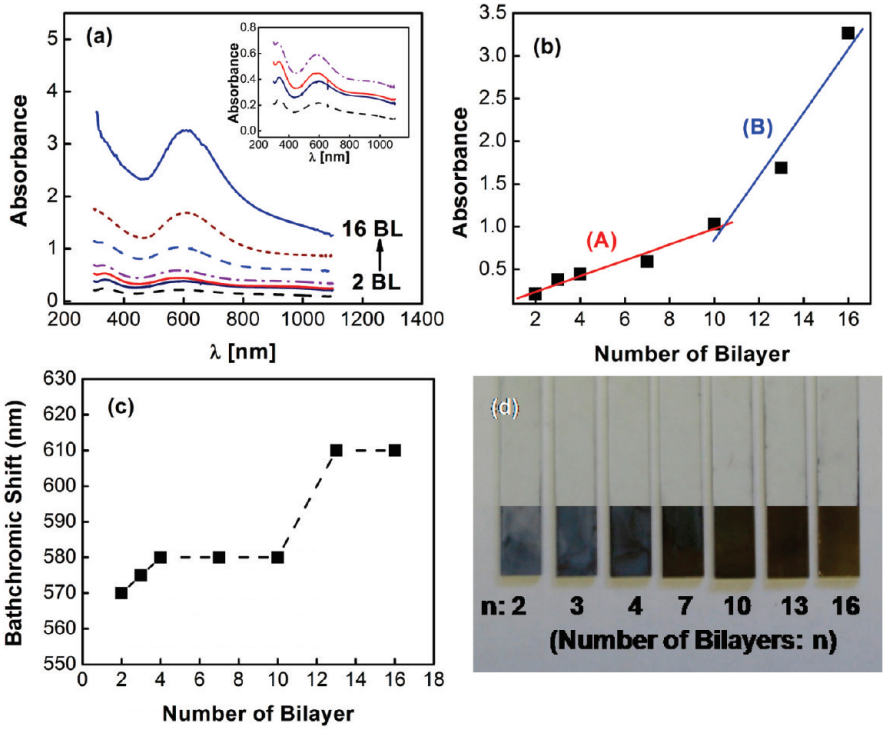

Figure 4. (a) UV/vis spectra of the AuNP/MWNT LBL film, (b) absorbance of the LBL films at surface plasmon band, (c) correlation between the number of bilayers and bathochromic shift on the LBL films, and (d) optical photographs of LBL film on the APTES/ITO electrodes.

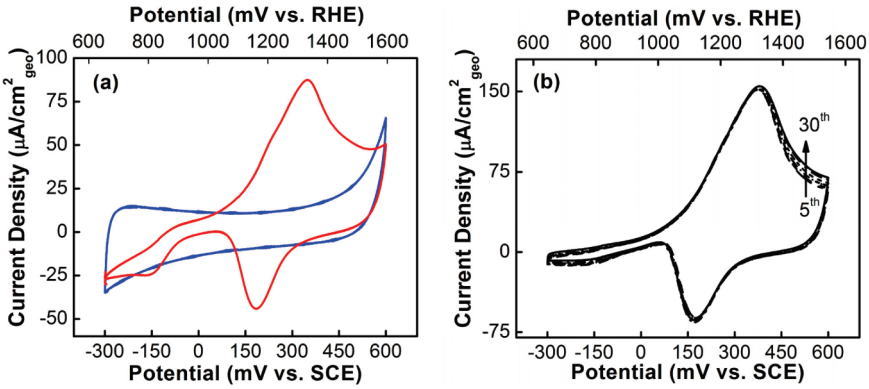

Figure 5. (a) Cyclic voltammetry (CV) of the 2-bilayer AuNP/MWNT thin film on the ITO electrode (solid, red) and the 10-bilayer MWNT/MWNT thin film on the ITO electrode (dot, blue) in the deaerated 1.0 M CH_3OH + 0.01 M KOH solution, (b) CV data the 4-bilayer AuNP/MWNT LBL film in the 5th, 10th, 15th, 20th, and 30th cycles.

note that the curve exhibits a dual linear region (i.e., two slopes) with an inflection point in the 10-bilayer film. The blue line B slope in the thicker film region from 10 to 16 bilayers is greater than that in the thinner bilayer film region from 2 to 10 bilayers (red line A). On the basis of the similar dual linear behavior observed in the thickness of the film with increased thickness per bilayer pair, this change in slope is due to the increased film thickness and more rapid film growth that occurs once surface coverage is reached between 7 and 13 bilayers, and uniform films are grown from the multilayer surface. In addition, Figure 4d shows changes in the colors with different numbers of bilayers. As the number of the bilayers increased, the stronger absorbance band is positioned in the longer wavelength region (panels a and c in Figure 4); aviolet (2, 3-bilayer films) and blue (4, 7, 10-bilayer films) and yellowish bulk gold metal (13, 16-bilayer films) color results.

The red line A in Figure 4b shows that the absorbance increases linearly, and drastically different surface plasmon resonance peaks are observed in Figure 4c with an increasing number of the bilayers. This surface plasmon band red shift results could have originated by dimensional (2D and/or 3D) interactions of AuNPs in the close proximity with each other but no aggregation is observed, as shown in Figures 1 and 2a; the oscillating electrons in one particle experience the electric field due to the oscillation of electrons in the closely packed surrounding AuNPs on the MWNT, and this leads to the appearance of a plasmon band attributed to the coupled plasmon absorbance of AuNPs.[62] The increase in the bathochromic shift between 10 and 13 bilayers is likely to be due to the increase in the AuNP agglomerate size,[63] as shown in Figures 2b and 4d. This is consistent with agglomeration of AuNPs as suggested from AFM images, for which the surface plasmon band is well-defined, and the reduced distance between AuNPs determines the shift of surface plasmon band toward higher wavelengths.[63,64]

AuNP/MWNT LBL Thin Films for Electrocatalytic Oxidation of Methanol in Alkaline Media. The cyclic voltammetry of an AuNP/MWNT LBL thin film on the APTES/ITO electrode measurements were first carried out in a 0.01 M KOH solution in the absence of methanol under a N_2 atmosphere (see the Supporting Information, Figure S3). Increasing oxidation current with an onset potential of ~1150 mV (vs RHE) was observed, which is indicative of adsorption of OH^- and subsequently the formation of surface oxides on AuNPs at higher potentials.[65,66] In the negative-going sweep, a reduction peak at ~1135 mV (vs RHE) was observed, which corresponded to the reduction of surface oxides and desorption of OH^- ions from AuNPs. The cyclic voltammograms of the AuNP/MWNT LBL film (solid, red) and a MWNT/MWNT LBL film[56] (dot, blue) on the APTES/ITO electrodes were obtained in a deaerated 1.0 M CH_3OH + 0.01 M KOH (Figure 5a). Large anodic wave voltammetry at 1295 mV (vs RHE) was observed for methanol oxidation in the 2-bilayer AuNP/MWNT LBL thin film on the APTES/ITO electrode. Such an electrochemical voltammetry response was not observed with the APTES/ITO and the 10-bilayer MWNT/MWNT thin film on the APTES/ITO electrodes in the same potential window in Figure 5a, which confirmed that AuNPs were responsible for the electrocatalytic activity for methanol oxidation in the AuNP/MWNT films. The increasing current at voltages greater than 1000 mV vs RHE in Figure 5a can be attributed to enhanced kinetics of methanol[65] oxidation promoted by adsorption of OH^- and the formation of surface oxide. With increasing potentials beyond the peak potential of ~1300 mV (vs RHE), the methanol oxidation rate was reduced due to surface oxide passivation while surface oxide coverage was reduced in the negative-going sweep, which led to increased methanol oxidation current.[65] Multiple cyclic voltammograms in Figure 5b show a stable electrochemical response signal upon extensive cycling.

Further investigation was made into the transport characteristics of methanol in the 3-bilayer film of AuNP/MWNT on the ITO electrode. The linear sweep

(62) Basu, S.; Ghosh, S. K.; Kundu, S.; Panigrahi, S.; Praharaj, S.; Pande, S.; Jana, S.; Pal, T. *J. Colloid Interface Sci.* **2007**, *313*, 724–734.
(63) Ung, T.; Liz-Marzan, L. M.; Mulvaney, P. *J. Phys. Chem. B* **2001**, *105*, 3441–3452.
(64) Liz-Marzan, L. M. *Langmuir* **2006**, *22*, 32–41.
(65) Assiongbon, K. A.; Roy, D. *Surf. Sci.* **2005**, *594*, 99–119.
(66) Chen, A. C.; Lipkowski, J. *J. Phys. Chem. B* **1999**, *103*, 682–691.

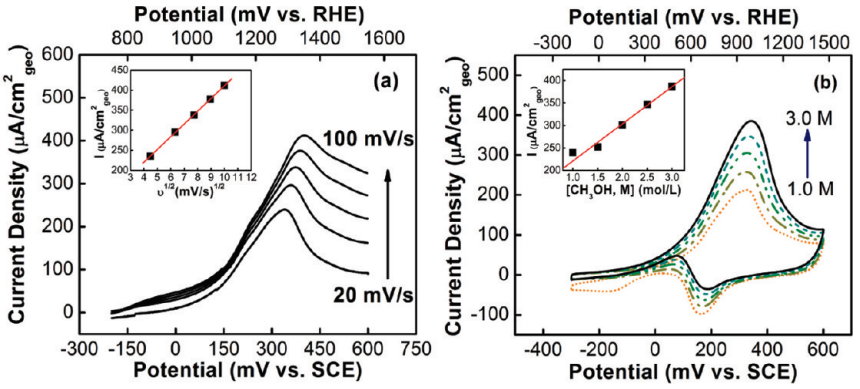

Figure 6. (a) Linear sweep voltammetry (LSV) of 3-bilayer AuNP/MWNT thin film on the ITO electrode with various scan rates of 20, 40, 60, 80, and 100 mV/s (υ) in 1.0 M CH_3OH + 0.01 M KOH solution, (b) cyclic voltammetry as a function of methanol concentration (1.0, 1.5, 2.0, 2.5, 3.0 M) in 0.01 M KOH.

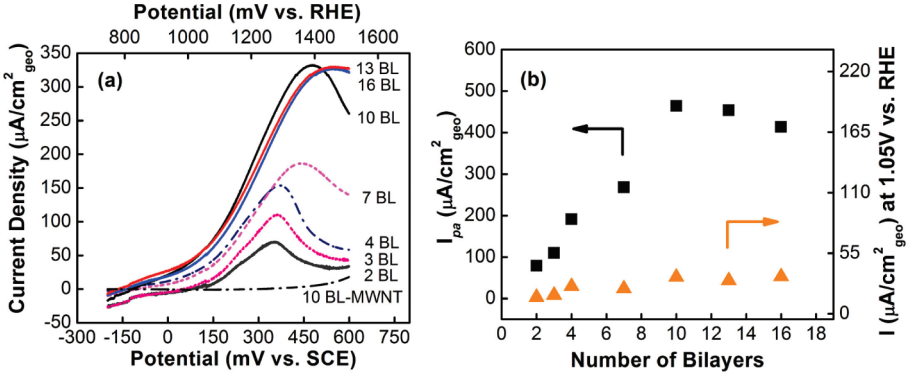

Figure 7. (a) Linear sweep voltammetry (LSV) of various bilayers (BL), (b) correlation of current density at 1050 mV (vs RHE) and number of bilayers, where the number of bilayers is denoted as BL in the graph.

voltammetry (LSV) shows that the anodic peak currents (i_{pa}) are linearly proportional to the square root of scan rates ($\upsilon^{1/2}$) (Figure 6a inset), revealing that the electrocatalytic oxidation of methanol by the AuNP/MWNT LBL thin films is a diffusion-controlled process[67] such as diffusion of methanol and KOH electrolyte in the thin films.

In the presence of methanol of different concentrations, the anodic peak current (i_{pa}) increases linearly with increasing methanol concentration, as shown in Figure 6b and inset. This observation suggests that electro-oxidation of methanol involves not only adsorbed OH^- on AuNPs but also solution OH^-.[65] In contrast, the peak current for the cathodic wave (i_{pc}) decreases with increasing methanol concentration, which could be attributed to reduced AuNP oxide coverage associated with increasing concentration of methanol on the positive-going sweep and thus decreased cathodic current for methanol oxidation and AuNP oxide reduction on the negative-going sweep. The opposite trend between the oxidation and reduction peak currents as a function of methanol concentration is suggestive of a catalytic mediation mechanism likely by surface Au oxide species.[37,68]

Figure 7 depicts linear sweep voltammograms for methanol oxidation with different numbers of bilayers of the AuNP/MWNT LBL films from the 2 bilayers to 16 bilayers. The 2-bilayer film shows a relatively sharp (full half-maximum width 100 mV) methanol oxidation peak at 1295 mV (vs RHE), which is in good agreement with the peak potentials of Au-coated fibrous mats[68] and thiolate-encapsulated Au−Pt NPs on a glass carbon electrode.[37] The oxidation peak width and peak potential increases with increasing number of bilayers, which may indicate increasing nonunformity in the kinetics of methanol oxidation in thicker film electrodes. The peak potential of the 2-bilayer film is about 150 mV greater negative potential value than that observed on the 13-bilayer AuNP/MWNT film on the ITO electrode (Figure 7a).

In addition, an inspection of linear sweep voltammograms reveals a systematic increase in the methanol oxidation current with increasing number of bilayers, where the peak current and the current at 1050 mV (vs RHE) normalized to the geometric area of AuNP/MWNT films are shown in Figure 7b. It should be noted that the current density increases linearly with the number of bilayers up to 10 bilayers. However, the 10, 13, and 16-bilayer film electrodes show nearly no change in the current density of electrocatalytic methanol oxidation. This inflection point at the 10-bilayer LBL film also corresponds with the plasmonic property of LBL films in Figure 4b. The limiting current of methanol electro-oxidation found for LBL films with 13 and 16 bilayers, with an electrode thickness of 160 and 200 nm, respectively, can be attributed

(67) Bard, A. J. F., L. R. Electrochemical Methods Fundamentals and Applications; Wiley: New York.
(68) Guo, B.; Zhao, S. Z.; Han, G. Y.; Zhang, L. W. *Electrochim. Acta* **2008**, *53*, 5174–5179.

to (1) the decrease in electrochemically active surface of AuNPs associated with nanoparticle agglomeration in the films; (2) diffusion control due to low electrode porosity as a result of high packing densities of AuNPs in the films. The AuNP core size was maintained in the thinner films including the 2, 4, 7, and 10 bilayers, whereas significant agglomeration of AuNPs was observed in thicker films as evidenced from the plasmonic properties and AFM images of the LBL films. Therefore, AuNPs in thinner film electrodes were better utilized for methanol oxidation than those in films thicker than 10 bilayers.

Conclusions

We used the layer-by-layer (LBL) method to assemble AuNP/MWNT thin films on an ITO substrate based on the electrostatic interaction between positively charged AuNPs and negatively charged functionalized MWNTs. The MWNTs in the structure of the LBL films presented a randomly entangled arrangement, which AuNPs were dispersed on MWNTs. A correlation was demonstrated between the film optical properties and the electrocatalytic methanol oxidation activity in alkaline solution as a function of number of bilayers.

The absorbance at the surface plasmon resonance and the methanol oxidation current increased linearly with increasing number of bilayers up to 10 bilayers. There was a change in the nature of AuNP/MWNT film growth from 10 to 13 bilayer pairs to a denser film structure, where AuNPs were found to aggregate and methanol oxide current stayed unchanged from 10 to 13 bilayers. These results demonstrate that the properties of nanostructured films can be tuned by tailoring the LBL nanoscale assembly conditions.

This work provides an alternative means to the preparation of metal nanoparticle/MWNT film with varying numbers of layers for electrochemical applications. In comparison to other reports of CNT incorporation into multilayers, this study is unique in the generation of an AuNP/MWNT film without added resistive organic material such as a polymer or dendrimer on the CNT or within the film. The high film electronic conductivity combined with well-dispersed NPs in the porous film electrode offer promise to the development of metal nanoparticle/MWNT (such as Pt and PtAu NPs[69]) electrodes for electrochemical energy conversion devices such as alkaline fuel cells and biosensors.

Acknowledgment. This work was supported in part by the MRSEC Program of the National Science Foundation under award number DMR 0819762. The authors thank Dr. Shuo Chen for help with TEM images. S.W.L. acknowledges a Samsung Scholarship from the Samsung Foundation of Culture.

Supporting Information Available: TEM images before and after carboxylic acid functional group surface-modified MWNT, UV/vis spectroscopy of AuNPs in pH 3.0 solution, and cyclic voltammetry (CV) of the 2-bilayer AuNPs/MWNTs thin film on the ITO electrode in the deaerated 0.01 M KOH solution (PDF). This material is available free of charge via the Internet at http://pubs.acs.org.

(69) Spendelow, J. S.; Wieckowski, A. *Phys. Chem. Chem. Phys.* **2007**, *9*, 2654–2675.